RESEARCH ARTICLE | APRIL 20 2026

Modeling interference of spin-waves and electromagnetic leakage in micron-scaled spin-wave transducers

Felix Kohl ; Björn Heinz ; Matthias Wagner ; Christoph Adelmann ; Florin Ciubotaru ;
Philipp Pirro

Appl. Phys. Lett. 128, 162401 (2026)
https://doi.org/10.1063/5.0308357

Applied Physics Letters ARTICLE pubs.aip.org/aip/apl

Modeling interference of spin-waves and electromagnetic leakage in micron-scaled spin-wave transducers

Cite as: Appl. Phys. Lett. **128**, 162401 (2026); doi: 10.1063/5.0308357
Submitted: 22 October 2025 · Accepted: 2 April 2026 ·
Published Online: 20 April 2026

View Online Export Citation CrossMark

Felix Kohl,[1,a)] Björn Heinz,[1] Matthias Wagner,[1] Christoph Adelmann,[2] Florin Ciubotaru,[2] and Philipp Pirro[1]

AFFILIATIONS

[1]Fachbereich Physik and Landesforschungszentrum OPTIMAS, Rheinland-Pfälzische Technische Universität Kaiserslautern-Landau, D-67663 Kaiserslautern, Germany
[2]imec, Kapeldreef 75, 3001 Heverlee, Belgium

[a)]Author to whom correspondence should be addressed: fkohl@rptu.de

ABSTRACT

The utilization of spin-wave transducers for radio frequency signal processing provides significant potential due to intrinsic tunability, scalability, and nonlinearity. However, signal interference with electromagnetic leakage can add further complexity for signal processing. Here, we experimentally identify the electromagnetic crosstalk (EM) as a major source of interference induced distortion and provide an analytic model based on the coherent interference of spin-waves and electromagnetic leakage to predict the impact on device operation. In addition, we test multiple transducer geometries to identify operational regimes and minimize the EM impact. Finally, the effect of nonlinear device operation on the interference is addressed, which is of relevance for the exploitation of the spin-waves intrinsic nonlinear traits.

In recent years, magnonics has been extended from fundamental research[1–3] to an increased focus on practical technological application of spin-waves.[2–7] In particular, due to their tunability, scalability, and accessible frequency range,[7] spin-waves offer many promising traits for next-generation signal processing and logic systems.[2,6,8–10] Accordingly, several approaches and prototypes for various use cases have been demonstrated in the recent past.[11–15] Many approaches are based on inductive excitation and detection of spin-waves using microstructured antennas on magnetic materials,[7,14,16,17] especially YIG, offering very low spin-wave attenuation.[18,19] Because of these qualities, similar but much larger devices have been the focus of extensive research efforts in the past.[20–27] However, as part of an ongoing trend toward miniaturization, recent work is primarily focused on microscale devices.[4–6,8,9] Although progress has been made in improving the efficiency of such spin-wave transducers,[28] the spin-wave antennas also couple inductively via the RF electric fields, giving rise to electromagnetic crosstalk (EM).[29,30] The resulting signal modulation, referred to as passband ripples, caused by this additional coupling has been observed in many studies but has been neglected due to different focus.[9,31,32] However, such distortions may impair signal integrity, emphasizing a need to investigate their cause and effects. In this paper, we present a simple modeling approach to describe the influence and effects of EM on signal transmission in micrometer-scaled spin-wave transducers. It is demonstrated that the interference of the spin-wave signal and EM induces passband ripples and modulations in group delay of the RF output. Relevant parameters influencing the modulation frequency, i.e., spin-wave dispersion and antenna spacing, are identified. Moreover, the magnitude is shown to depend strongly on the relative magnitudes of spin wave and EM signals. In the experiments, the amplitude ratio and consequently the occurrence of passband ripples depend on the antenna layout and operation power level, and their influence can be minimized by careful design of the transducers depending on the use case.

In a spin-wave transducer, the dynamic Oersted fields of the driving antenna excite spin-waves in an adjacent magnetic material. These spin-waves then propagate through the magnet and eventually reach the detection antenna. There, the dynamic magnetic fields of the spin-waves induce an oscillating voltage in the antenna.[7,16,28,33] A simple analytical model for calculating this coupling is given in Ref. 34. According to this model, the antenna's self-inductance L_m induced by the spin-waves and the mutual inductance $\mathcal{M}$ mediated by propagating spin-waves can be expressed as

$$L_{\mathrm{m}} = \mu_0 t l \int \mathbf{h}_a^T(k)\chi(\omega(k))\mathbf{h}_a^*(k)\frac{dk}{2\pi}, \quad (1)$$

$$\mathcal{M} = \mu_0 t l \int e^{ikD}\mathbf{h}_a^T(k)\chi(\omega(k))\mathbf{h}_a^*(k)\frac{dk}{2\pi}, \quad (2)$$

for an antenna of length l on a magnet of thickness t and an antenna pair of distance D. In the expressions, $\chi(\omega(k))$ represents the frequency-dependent dynamic susceptibility of the magnet and $\mathbf{h}_a^*(k)$ the wave-vector-dependent Fourier amplitude of the dynamic antenna field. The expressions used for these quantities to calculate the total transmission signal are outlined in the supplementary material. The resulting spectrum of spin-wave transmission is described, e.g., in Ref. 28. A direct comparison of both expressions reveals they only differ by a complex phase term, which describes the phase accumulation as they propagate to the detection antenna. The Gilbert losses are fully included in the complex susceptibility $\chi(\omega(k))$.[35]

In the experiment, spin-wave wavelengths are on the order of micrometers, well below the wavelength of microwave radiation in the GHz range. Considering an antenna distance of $D = 50\ \mu$m, a considerable spin-wave phase accumulation is therefore expected. Additionally, the antenna emits a near-field electromagnetic field toward the detection antenna, although phase accumulation is negligible at such short distances. Based on induction law, EM generates a voltage in the detection antenna too, and the superposition with the spin-wave contribution is measured. Since the accumulated spin-wave phase is wave-vector dependent, the relative phase between the two voltages varies with frequency. When sweeping the frequency, points of constructive (orange in Fig. 1) and destructive interference (red in Fig. 1) occur, resulting in a modulation of the measured signal magnitude. The lower right inset of Fig. 1 shows a typical dispersion relation for YIG films with thickness in the micrometer range, dominated by magnetostatic contributions (here: Damon–Eshbach). Due to the nonlinear spin-wave dispersion relation, the resulting oscillations in signal magnitude are not constant but frequency-dependent.

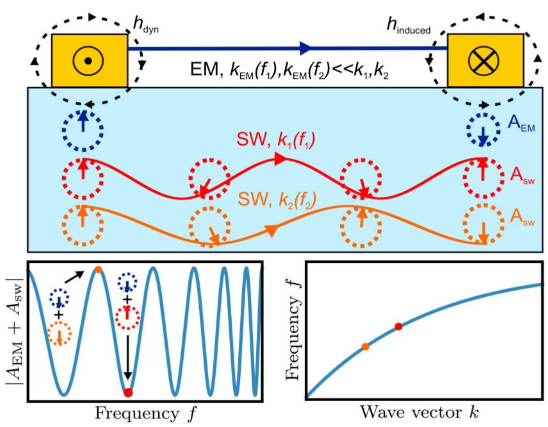

FIG. 1. Schematic illustration of signal transmission by EM and spin-waves. Spin-wave phase accumulation is strongly dispersive. The total measurement signal includes the spin-wave and EM signal. The resulting interference of both signal amplitudes depicted in the left sub-panel reveals frequency-dependent modulation. As the spin-wave dispersion, depicted in the right sub-panel, is not linear, the modulation period in the left sub-panel changes with frequency.

Constructive interference occurs, when the spin-wave phase is $k(f)\cdot D = 2\pi n$ ($n = 0, 1, 2, \ldots$) relative to the EM phase. If the dispersion is steep, i.e., at low wave-vectors, the frequency spacing between points of the spin-wave dispersion of relative phase shift $\Delta k \cdot D = [k(f_2) - k(f_1))]\cdot D = 2\pi$ is large. For larger wave-vectors, the dispersion flattens noticeably. Consequently, the same $\Delta k \cdot D$ is achieved for smaller frequency steps, and the oscillation period decreases. Simultaneously, increasing propagation distance D results in faster phase accumulation and shorter oscillation periods.

To model the superposition, we adapt the equivalent circuit for the two-port network from Refs. 28 and 36, as shown in Fig. 2(a). It describes the two-port network as a series connection of the electrical properties of the antennas including the inductive coupling via the EM and the contributions due to the spin-wave excitation [see Eqs. (1) and (2)]. Using this adapted circuit, the scattering matrix can be calculated, as shown in the supplementary material. Exemplary, a pair of GS antennas with a spacing of 50 μm identical to the experiment is considered. The antenna dimensions and excitation efficiencies are presented in the supplementary material. The external field is 143 mT, and the impedance of the EM is set to be frequency-independent 2Ω. This value is close to the mutual impedances measured for the off-resonant background in the experiment. The calculated transmission spectra in forward and backward direction are shown in Fig. 2(b). There, black curves represent the spectrum without crosstalk, while the colored curves include the EM. The pronounced difference between the forward direction S_{21} (solid) and the backward direction S_{12} (dashed) is caused by the nonreciprocal excitation and detection efficiency in the Damon–Eshbach geometry, that is caused by the either constructive (forward direction) or destructive interference (backward direction) of spin-waves driven by the out-of-plane and in-plane antenna field components.[8,28,37,38] For both directions, the inclusion of the EM induces a periodic modulation in signal magnitude, referred to as passband ripple. Due to flattening of the dispersion relation (see Fig. 1), the modulation period decreases toward higher frequencies. Both transmission directions allow differentiation between two modulation regimes: For strong spin-wave transmission (S_{21}, red), the spin-wave signal is significantly larger than the EM, leading to a modulation of the spin-wave envelope. In contrast, for weak spin-wave transmission (S_{12}, blue), EM dominates and is modulated by the spin-waves.

The interference of both contributions also affects phase and group delay of the signal. The latter is defined as the frequency derivative of the phase, providing a measure of the propagation time and phase coherence when passing the transducer,

$$\tau = -\frac{\mathrm{d}\phi(\omega)}{\mathrm{d}\omega}. \quad (3)$$

Please note a considerable phase is accumulated only in the spin-wave band due to the small transducer spacing relative to EM wavelength. To illustrate the effects of the interference, Fig. 2(c) displays the phase difference between the undisturbed and the modulated case for a strong spin-wave transmission within the spin-wave band. As in the magnitude, the phase shows a periodic modulation, growing stronger toward the edges of the spin-wave band (as the spin-wave transmission becomes weaker). The impact on the group delay for this case, due to its definition as the derivative of the phase to the frequency, is even more pronounced as highlighted in the bottom panel. The

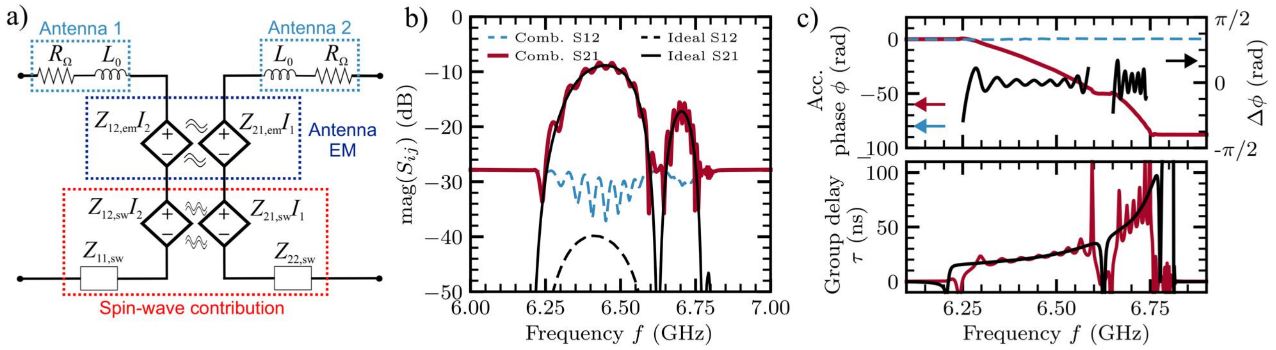

FIG. 2. (a) Illustration of the combined network including the EM used to calculate the signal transmission. (b) Calculated transmission spectra for GS antenna on 500 nm thick YIG film with $M_s = 158.3$ kA/m and $A_{ex} = 3.5$ pJ/m in 143 mT external field for forward (S_{21}, solid lines) and backward transmission (S_{12}, dashed lines). Shown in black is the ideal case of zero EM, and colored lines refer to a real EM of 2 Ω. Including the EM introduces a periodic modulation. (c) Top panel: Unwrapped phase accumulation for S_{21} (red) and S_{12} (blue) including the EM. The spin-wave phase accumulation dominates. Shown in black is the difference to the pure spin-wave phase accumulation, revealing the periodic modulation by interference with the EM. Bottom panel: Group delay for S_{21} with (red) and without (black) EM. Here, the same modulation appears.

impact on variations of the EM level, antenna spacing, and external bias field is discussed in the supplementary material. The presented model illustrates that the EM influence on the phase poses challenges for phase-sensitive applications. Following the description of the origins and implications of this interference, the anticipated effects are examined experimentally as follows.

Propagating spin-wave spectroscopy (PSWS) measurements are performed[16,19,33,39] using an electromagnet and a two-port VNA. The sample is contacted by 150 μm-pitch ground-signal-ground (GSG) RF probes. Before the measurements, a short-open-load-through calibration is performed using an on-chip calibration substrate. An input RF power of −25 dBm was selected to ensure operation in the linear spin-wave excitation regime.

The structures under test are fabricated on 500 nm thick YIG films on a 500 μm thick GGG substrate. Using UV lithography, the spin-wave antennas made from 10/250 nm titanium/gold are fabricated onto a 50 nmSiO_2 film deposited onto the YIG film using chemical vapor deposition at 250 °C. The spacer prevents direct contact between metal and YIG. Overall, three types of antennas are produced to investigate the impact of the antenna layout [see Fig. 4(a)]: a ground-signal (GS), a ground-signal-ground (GSG), and a GSGS antenna (two periods of the GS design). For all antennas, the dimensions, around 2 μm, and excitation efficiencies are presented in the supplementary material.

To disentangle the contributions of spin-waves and EM, a method to filter the experimental data is required, which is presented in the following. The impact of antenna shape and the power dependence are considered thereafter.

In the experiment, the frequency-dependent transmission is measured from 2 to 14 GHz in 2 MHz steps. The harmonic frequency grid allows conversion of the frequency spectrum into an artificial time-domain response following the method from Ref. 40. In the following, a pair of GS antennas with $D = 50$ μm separation [see inset Fig. 3(a)] is considered exemplary. The calculated timetrace in Fig. 3(a) represents the output voltage in response to a Dirac impulse excitation at $t = 0$.[40] This representation differs from the measured

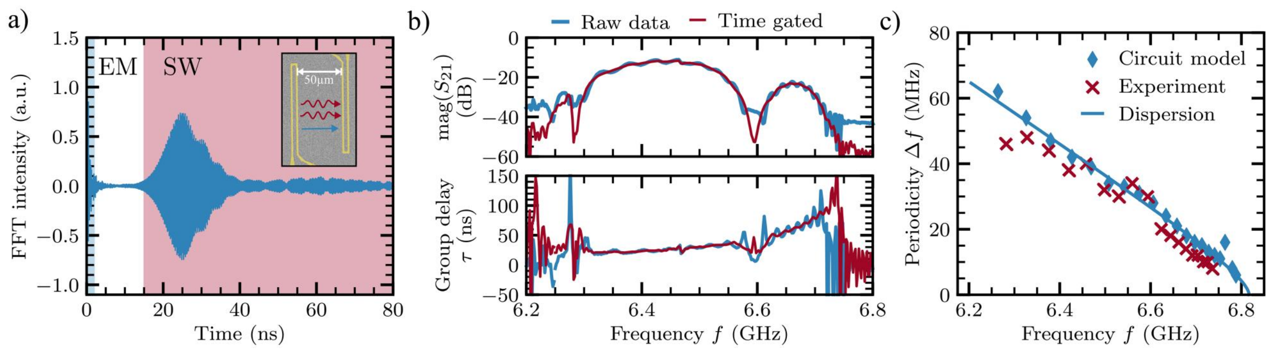

FIG. 3. (a) Timetrace calculated from the frequency spectrum measured in (b) for the GS antenna at 143 mT external field. Times corresponding to the EM and the spin-waves are shaded. The inset shows a scanning-electron-microscope image of the GS antenna pair including an illustration of spin-waves and EM. (b) Measured (blue) transmission spectrum (top) and group delay (bottom) along with the EM-filtered spectrum (red). Excluding the EM contribution removes the periodic modulation from the signal. (c) Periodicity of the modulation obtained using the circuit model with the same parameters as in the experiment (blue diamonds) along with the periodicity calculated from the dispersion relation (blue). Red crosses mark the periodicity extracted from the experiment on the GS antenna.

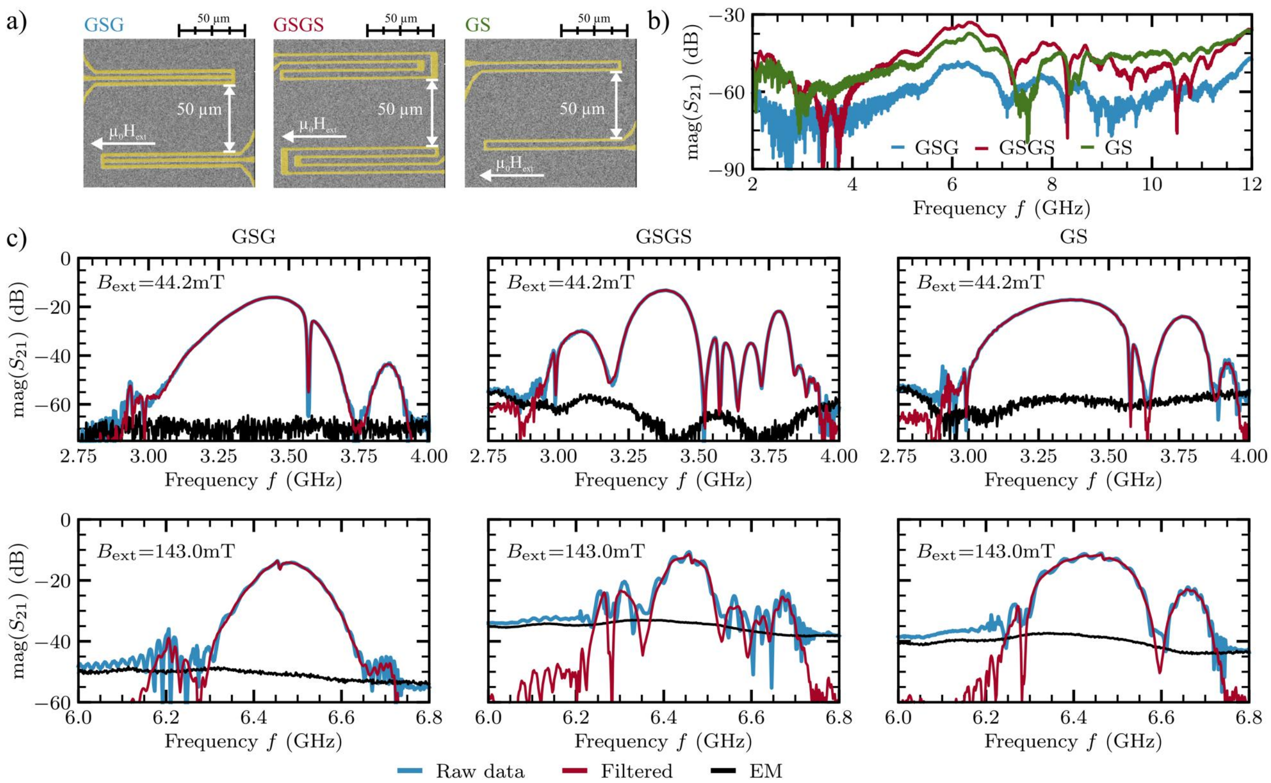

FIG. 4. (a) Colored scanning-electron microscope images of all antennas investigated. (b) Transmission spectra of the EM acquired for all antennas at zero external field. Depending on antenna layout, strong differences in EM level arise. Consequently, the antenna layout will impact on the magnitude of the EM induced modulation. (c) Measured and filtered transmission magnitudes of all antenna types at two different external field values along with the off-resonant EM magnitude. For all antennas, time gating by excluding the first 2.5 ns removes the modulations from the transmission spectra. The different shape of transmission spectra is attributed to the differences in antenna field wave-vector spectra. The antenna with the strongest EM level shows the strongest modulation, while for the GSG, the influence is only weak.

$S_{21}(f)$ continuous wave (CW) excitation yet provides insights into the temporal evolution of signal transmission. Owing to the method of Ref. 40, the timetrace is real-valued.

Figure 3(a) shows that the largely different propagation velocities yield a temporal separation: Electrical crosstalk, propagating with the speed of light, arrives almost immediately at the output antenna, while spin-waves—with group velocities of kilometers per second—arrive after about 20 ns. Using this separation, the EM influence is filtered out by setting the first 2.5 ns to zero [blue region in Fig. 3(a)]. The modified timetrace is then transformed back into the frequency domain, resulting in a transmission spectrum without EM contribution. The procedure, referred to as time gating, applied to the S_{12} trace is shown in the supplementary material.

Figure 3(b) compares the raw and timegated spectra. The raw spectrum exhibits passband ripples, while, after time gating, these modulations vanish, confirming their origin in the interference of spin-waves and EM. Accordingly, filtering the EM also removes the oscillations in the group delay, as shown in the bottom panel. For comparison, the oscillation periodicities extracted from the experiment and a calculation using the measured off-resonant EM are plotted in Fig. 3(c) along with values obtained from the frequency difference of wave-vector pairs with difference in accumulated phase of 2π using the dispersion relation: $\Delta k = 2\pi/D$. The agreement between the measured periodicities and both calculation approaches confirms the validity of the modeling. In the supplementary material, the back-action on the input antenna (S_{11}) is presented along a discussion on purely spin-wave coupling induced modulations.

Having confirmed the cause of the passband ripple, the influence of the antenna layout is considered. Based on the interference model, modulation depends strongly on EM magnitude between both antennas and thus also on the shape of the whole transducer. Therefore, three different transducer layouts, as shown in Fig. 4(a), are compared regarding EM magnitude. The measured EM at zero external field is shown in Fig. 4(b). Across the frequency range, the GSG antenna (blue) exhibits the lowest level of crosstalk, while either the GS (green) or GSGS (red) antenna alternately exhibit the strongest EM. Consequently, the passband ripples are predicted to vary depending on antenna type and frequency. A numerical comparison of the expected EM levels arising from the varying transducer layouts is presented in the supplementary material. Please note that all antenna types exhibit an increased EM between 5.5 and 7 GHz. Due to the overall low levels in EM, even small changes in the environment after the calibration[41] and metallization in the probe shadow[42] can influence the shape of the measured EM dependence.

Figure 4(c) presents the measured spin-wave transmission spectra in distinct frequency ranges for the three antennas. The

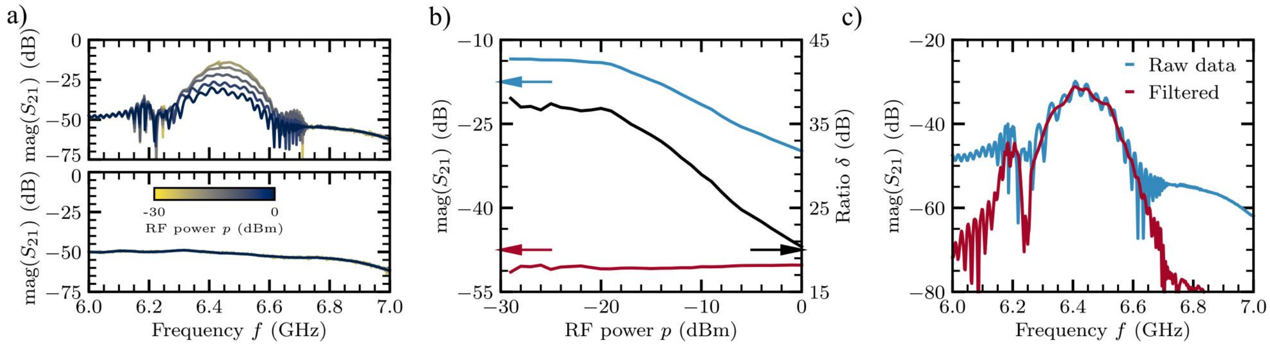

FIG. 5. (a) Measured transmission spectra for the GSG antenna at 142 mT (top) and 0 mT (bottom) external field for varying input power. The spin-wave signal depends on the input power for high powers, while the EM is linear across the whole range. (b) Extracted transmission magnitudes as a function of input power for maximum spin-wave transmission and the corresponding EM magnitude. The ratio is shown in black. Due to the spin-wave nonlinearity, the ratio decreases at high power. (c) Measured transmission spectrum for 0 dB input power before and after filtering the first 2.5 ns.

pronounced dips in the GS and GSG spectra do not result from interference but are due to hybridization gaps between the spin-wave surface mode and higher-order thickness modes, as already observed on similar transducers.[28] At these points in the dispersion relation, both modes form an avoided crossing leading to a small gap in the frequency band, where spin-waves cannot propagate. Consequently, the transmission magnitude drops around these points in the spectrum. For the measurements shown in Fig. 4(c), these dips are located at 3 and 3.55 GHz for the top row and around 6.3 and 6.45 GHz for the bottom row. Within the lower frequency range, the EM is found to be minimal across all antenna types. Consequently, no pronounced modulations are evident in the raw spectra for all antennas. However, for frequencies of approximately 6 GHz, the EM levels are high. Consequently, all three antennas, including the GSG antenna, exhibit the previously identified modulations, which can be eliminated by time gating. The crosstalk magnitudes depicted in Fig. 4(b) reveal the strongest modulation for the meander antenna, while it is least evident for the GSG antenna. This comparison highlights the need to adapt the antennas to the intended operation frequency range to ensure maximum suppression of passband ripple.

In the previous measurements, the input power was always kept in the linear regime. Within this regime, the ratio of spin-wave to EM contribution is constant with respect to variation of RF input power. As the nonlinear regime is desired for some use cases, i.e., frequency-selective limiting,[9] the impact on the passband ripples is explored using the GSG antenna. In the nonlinear regime, additional spin-wave losses arise from scattering processes in the spin-wave system, decreasing the relative spin-wave magnitude,[9,28] while the EM scales linear. In the experiment, the transmission magnitude is measured relative to the input. A linear power dependence therefore translates to constant transmission magnitude, while the spin-wave attenuation leads to decreased transmission. Accordingly, only for the spin-wave transmission, but not the EM, a relative weakening is expected, as observed in Fig. 5(a). Importantly, the passband ripples are observed to increase with input power in the spin-wave nonlinear regime.

The extracted signal magnitudes are plotted at the frequency of maximum spin-wave transmission in Fig. 5(b). For the magnitude of the spin-waves, the influence of the electrical crosstalk was first excluded by time gating. The spin-waves (blue) show constant power level in the linear regime, which decreases toward high powers. For the EM (red), this curve is constant for all powers. Accordingly, the ratio of both signal levels (black) is lower for high powers than for low powers, leading to a strong increase in modulation. To check whether the observed modulation for high powers is induced by the described mechanism, Fig. 5(c) shows the measured spectrum at 0 dBm before and after the time gating. As for the linear measurements, the modulation is filtered out by excluding the EM. This shows the influence of the EM is always present and can effectively be minimized by a large magnitude ratio. This behavior is consistent with previous studies,[9,31] also observing similar spectral features, underlining the importance of improving the efficiency of microscale spin-wave devices while reducing interference effects.

In this work, we presented a simple analytic description of the interaction between spin-waves and EM inside integrated micrometer-sized spin-wave transducers. The interference of both is found to induce passband ripples as well as distortions in phase and group delay depending on the relative magnitude between both. The ratio is observed to be power-dependent due to the nonlinear saturation of spin-wave transmission magnitude at high power levels. It is important to note here, this interference effect has been studied only in continuous wave (CW) operation. For pulsed excitation, with a pulse duration shorter than the propagation time of the spin-waves, there is no temporal overlap, therefore no interference between the EM and the spin-waves excited by the same pulse. However, an interference between pulses in a pulse train might occur. In CW operation, suppression of the interference is possible by the reduction of the EM magnitude, i.e., by choosing antenna layouts with reduced EM. This work lays an important foundation for the characterization and reduction of unwanted passband ripple and phase distortion in integrated magnonic devices on the micrometer-scale.

See the supplementary material for information about the YIG characterization and the antenna structures. Additionally, calculations varying the parameters forming the passband ripples along explanations of the back-action on the driving antenna and an intrinsic source of the passband ripples are included. Electromagnetic simulations of the EM are also included.

The authors thank Johan Vanbellingen and the imec cleanroom technical support team for their assistance with device fabrication.

Financial support by the EU Horizon Europe research and innovation program within the projects "MandMEMS" (Grant No. 101070536) and "SPIDER" (Grant No. 101070417) is gratefully acknowledged.

AUTHOR DECLARATIONS

Conflict of Interest

The authors have no conflicts to disclose.

Author Contributions

Felix Kohl: Conceptualization (lead); Formal analysis (lead); Investigation (lead); Methodology (lead); Visualization (equal); Writing – original draft (lead). **Björn Heinz**: Conceptualization (supporting); Formal analysis (supporting); Investigation (supporting); Project administration (supporting); Visualization (supporting); Writing – original draft (supporting); Writing – review & editing (lead). **Matthias Wagner**: Conceptualization (supporting); Formal analysis (supporting); Investigation (supporting); Project administration (supporting); Visualization (supporting); Writing – original draft (supporting); Writing – review & editing (equal). **Christoph Adelmann**: Project administration (supporting); Resources (supporting); Writing – review & editing (supporting). **Florin Ciubotaru**: Project administration (supporting); Resources (lead); Writing – review & editing (supporting). **Philipp Pirro**: Funding acquisition (lead); Project administration (equal); Supervision (lead); Writing – review & editing (supporting).

DATA AVAILABILITY

The data that support the findings of this study are available from the corresponding author upon reasonable request.

REFERENCES

[1]M. R. Schweizer, F. Kühn, V. S. L'vov, A. Pomyalov, G. von Freymann, B. Hillebrands, and A. A. Serga, Appl. Phys. Lett. **124**, 092402 (2024).
[2]B. Flebus, D. Grundler, B. Rana, Y. Otani, I. Barsukov, A. Barman, G. Gubbiotti, P. Landeros, J. Akerman, U. Ebels, P. Pirro, V. E. Demidov, K. Schultheiss, G. Csaba, Q. Wang, F. Ciubotaru, D. E. Nikonov, P. Che, R. Hertel, T. Ono, D. Afanasiev, J. Mentink, T. Rasing, B. Hillebrands, S. V. Kusminskiy, W. Zhang, C. R. Du, A. Finco, T. van der Sar, Y. K. Luo, Y. Shiota, J. Sklenar, T. Yu, and J. Rao, J. Phys.: Condens. Matter **36**, 363501 (2024).
[3]P. Pirro, V. I. Vasyuchka, A. A. Serga, and B. Hillebrands, Nat. Rev. Mater. **6**, 1114 (2021).
[4]M. Cocconcelli, S. Tacchi, R. Erdélyi, F. Maspero, A. Del Giacco, A. Plaza, O. Koplak, A. Cattoni, R. Silvani, M. Madami, A. Papp, G. Csaba, F. Kohl, B. Heinz, P. Pirro, and R. Bertacco, Phys. Rev. Appl. **22**, 064063 (2024).
[5]Q. Wang, R. Verba, K. Davídková, B. Heinz, S. Tian, Y. Rao, M. Guo, X. Guo, C. Dubs, P. Pirro, and A. V. Chumak, Nat. Commun. **15**, 7577 (2024).
[6]Q. Wang, M. Kewenig, M. Schneider, R. Verba, F. Kohl, B. Heinz, M. Geilen, M. Mohseni, B. Lägel, F. Ciubotaru *et al.*, Nat. Electron. **3**, 765 (2020).
[7]K. O. Levchenko, K. Davídková, J. Mikkelsen, and A. V. Chumak, IEEE Trans. Magn. (published online 2026).
[8]Y. Li, T.-H. Lo, J. Lim, J. E. Pearson, R. Divan, W. Zhang, U. Welp, W.-K. Kwok, A. Hoffmann, and V. Novosad, Appl. Phys. Lett. **123**, 022406 (2023).
[9]K. Davídková, K. Levchenko, F. Bruckner, R. Verba, F. Majcen, Q. Wang, M. Lindner, C. Dubs, V. Vlaminck, J. Klíma, M. Urbánek, D. Suess, and A. Chumak, Phys. Rev. Appl. **23**, 034026 (2025).
[10]T. Devolder, Phys. Rev. Appl. **20**, 054057 (2023).
[11]D. Breitbach, M. Bechberger, B. Heinz, A. Hamadeh, J. Maskill, K. O. Levchenko, B. Lägel, C. Dubs, Q. Wang, R. Verba, and P. Pirro, Appl. Phys. Lett. **124**, 092405 (2024).
[12]Q. Wang, G. Csaba, R. Verba, A. V. Chumak, and P. Pirro, Phys. Rev. Appl. **21**, 040503 (2024).
[13]Á. Papp, W. Porod, and G. Csaba, Nat. Commun. **12**, 6422 (2021).
[14]X. Du, M. H. Idjadi, Y. Ding, T. Zhang, A. J. Geers, S. Yao, J. B. Pyo, F. Aflatouni, M. Allen, and R. H. Olsson III, Nat. Commun. **15**, 3582 (2024).
[15]X. Han, H. Wu, and T. Zhang, Appl. Phys. Lett. **125**, 020501 (2024).
[16]V. Vlaminck and M. Bailleul, Phys. Rev. B **81**, 014425 (2010).
[17]S. Dai, S. A. Bhave, and R. Wang, IEEE Trans. Ultrason., Ferroelectr., Freq. Control **67**, 2454 (2020).
[18]C. Dubs, O. Surzhenko, R. Linke, A. Danilewsky, U. Brückner, and J. Dellith, J. Phys. D **50**, 204005 (2017).
[19]H. Qin, S. J. Hämäläinen, K. Arjas, J. Witteveen, and S. van Dijken, Phys. Rev. B **98**, 224422 (2018).
[20]P. Emtage, J. Appl. Phys. **49**, 4475 (1978).
[21]J. Sethares, IEEE Trans. Microwave Theory Tech. **27**, 902 (1979).
[22]J.-P. Castera, J. Appl. Phys. **55**, 2506 (1984).
[23]D. Webb, C. Vittoria, P. Lubitz, and H. Lessoff, IEEE Trans. Magn. **11**, 1259 (1975).
[24]W. Ishak, Proc. IEEE **76**, 171 (1988).
[25]R. Marcelli, P. De Gasperis, M. Rossi, and M. Guglielmi, IEEE Trans. Magn. **27**, 5471 (1991).
[26]S. V. Zagriadski, J. Choi, and H. Kim, IEEE Trans. Microwave Theory Tech. **51**, 744 (2003).
[27]S. Bajpai, R. Weinert, and J. Adam, J. Appl. Phys. **58**, 990 (1985).
[28]F. Kohl, B. Heinz, Á. Papp, R. Erdélyi, G. Csaba, and P. Pirro, "Identification and minimization of losses in microscaled spin-wave transducers," arXiv:2505.08656 (2025).
[29]J. Greil, M. Golibrzuch, M. Kiechle, Á. Papp, V. Ahrens, G. Csaba, and M. Becherer, IEEE Trans. Magn. **59**, 1 (2023).
[30]A.-C. Bunea, F. Ciubotaru, F. Meng, C. Adelman, O.-G. Profirescu, and D. Neculoiu, Rom. J. Inf. Sci. Technol. **28**, 125 (2025).
[31]M. Song, J. Lim, W. Zhang, D. A. Bozhko, R. Divan, A. Hoffmann, K.-J. Kim, V. Novosad, and Y. Li, npj Spintronics **3**, 12 (2025).
[32]D. Schmoll, A. A. Voronov, R. O. Serha, D. Slobodianiuk, K. O. Levchenko, C. Abert, S. Knauer, D. Suess, R. Verba, and A. V. Chumak, Phys. Rev. B **111**, 134428 (2025).
[33]M. Bailleul, D. Olligs, and C. Fermon, Appl. Phys. Lett. **83**, 972 (2003).
[34]F. Vanderveken, V. Tyberkevych, G. Talmelli, B. Sorée, F. Ciubotaru, and C. Adelmann, Sci. Rep. **12**, 3796 (2022).
[35]M. Sushruth, M. Grassi, K. Ait-Oukaci, D. Stoeffler, Y. Henry, D. Lacour, M. Hehn, U. Bhaskar, M. Bailleul, T. Devolder, and J.-P. Adam, Phys. Rev. Res. **2**, 043203 (2020).
[36]R. Erdélyi, G. Csaba, L. Maucha, F. Kohl, B. Heinz, J. Greil, M. Becherer, P. Pirro, and Á. Papp, Sci. Rep. **15**, 9806 (2025).
[37]M. Kostylev and A. Stashkevich, J. Magn. Magn. Mater. **484**, 329 (2019).
[38]P. Deorani, J. H. Kwon, and H. Yang, Curr. Appl. Phys. **14**, S129 (2014).
[39]M. Vaňatka, K. Szulc, O. Wojewoda, C. Dubs, A. V. Chumak, M. Krawczyk, O. V. Dobrovolskiy, J. W. Kłos, and M. Urbánek, Phys. Rev. Appl. **16**, 054033 (2021).
[40]T. Devolder, G. Talmelli, S. Ngom, F. Ciubotaru, C. Adelmann, and C. Chappert, Phys. Rev. B **103**, 214431 (2021).
[41]M. Seelmann-Eggebert, M. Ohlrogge, R. Weber, D. Peschel, H. Maßler, M. Riessle, A. Tessmann, A. Leuther, M. Schlechtweg, and O. Ambacher, IEEE Trans. Microwave Theory Tech. **63**, 2335 (2015).
[42]G. N. Phung, F. J. Schmückle, R. Doerner, B. Kähne, T. Fritzsch, U. Arz, and W. Heinrich, IEEE Trans. Microwave Theory Tech. **67**, 1892 (2019).